Reversible and irreversible β-relaxations in metallic glasses

R. Zhao [1,2] H. Y. Jiang,[1] P. Luo,[1,*] L. Q. Shen,[1,3] P. Wen,[1,3] Y. H. Sun,[1,2,3] H. Y. Bai,[1,2,3] and W. H. Wang[1,2,3,†]

[1]*Institute of Physics, Chinese Academy of Sciences, Beijing 100190, China*
[2]*Center of Materials Science and Optoelectronics Engineering, University of Chinese Academy of Sciences, 100049 Beijing, China*
[3]*Songshan Lake Materials Laboratory, Dongguan, Guangdong 523808, China*

The localized β-relaxation process is critical for understanding the complex dynamics and controlling the properties of glasses. However, the β-relaxation in most metallic glasses only appears in a form of excess wing or shoulder in dynamic mechanical spectra while the underlying mechanism of the β-relaxation remains elusive. In the present work, the β-relaxation of metallic glasses is systematically studied by calorimetry where the glass-transition temperature (T_g) is resolved. The key finding is that the long-time sub-T_g annealing induces an endothermic peak upon heating prior to T_g with an activation energy of $\sim 26 RT_g$. By using an annealing-scanning-annealing thermal protocol, we show that this distinct endothermic sub-T_g peak is a reversible β-relaxation, indicating that the β-relaxation has both reversible and irreversible parts, which can be refined by the combination of calorimetry and the designed thermal protocol. The results might deepen our understanding of relaxation and the aging of metallic glasses.

I. INTRODUCTION

The widespread use of glasses is limited by the lack of a detailed understanding of their relaxation processes which results in the property deterioration in aging [1,2]. The primary α-relaxation, associated with large-scale collective atomic motions, is almost frozen below the glass-transition temperature (T_g) [3], while the secondary β-relaxation, concerning localized atomic/molecular rearrangements, persists in the glassy state and connects to the mechanical properties of glasses [4–10]. The presence of β-relaxations is universal for all glassy materials [11,12], but the underlying mechanisms are not fully understood. Metallic glasses (MGs) have unique mechanical and functional properties yet simple atomic structures, providing a model system for the study of β-relaxation and its relevance to the properties of glasses [11–15]. For example, β-relaxation is closely related to the ductility of MGs [6,10] and has the same activation energy as the flow units responsible for the localized deformation events [6]. Recent studies on probing the extremely slow flow behaviors of MGs revealed that in the as-cast MG, the flow is usually fast, whereas in the preannealed samples, the flow becomes much slower and follows a stretched exponential function with a magic exponent of 3/7 [16]. Stress relaxation appears as a one-step process in the as-cast MGs, whereas it becomes a two-step process in the preannealed MGs [17,18]. Numerical simulations found that the presence of extra cascade process of large groups of atoms is more frequently observed in the fast-quenched MGs than in the slowly quenched MGs [19]. Therefore, these results imply that there are contrasting relaxation behaviors between the as-cast and the preannealed MGs.

The β-relaxation in MGs is normally detected by dynamic mechanical analysis (DMA). However, in most MGs, the β-relaxation only appears in a form of excess wing or shoulder in DMA, which is not so sensitive to the minor changes of this localized relaxation mode [11,14]. In this work, we show that the differential scanning calorimetry (DSC) can effectively detect the β-relaxation of the preannealed MGs, and the critical finding is that the localized β-relaxation in MGs includes both reversible and irreversible parts. Isothermal annealing can separate the dynamic modes of β-relaxation, decoupling two processes of β-relaxation. This work provides deep insights into the features and mechanisms of the β-relaxation as well as their relationship with microstructure and properties in MGs.

II. EXPERIMENTAL DETAILS

Three kinds of MG compositions of $La_{60}Ni_{15}Al_{25}$, $Zr_{50}Cu_{40}Al_{10}$, and $(La_{0.8}Ce_{0.2})_{68}Al_{10}Cu_{20}Co_2$ (at. %) were fabricated by melt spinning in an argon atmosphere into thin ribbons. The T_g of these MGs, measured at $40\,K\,min^{-1}$, are 485, 702, and 378 K, respectively. The samples were sealed in quartz tubes filled with high-purity argon atmosphere to prevent oxidation during annealing. The amorphous nature of the samples before and after annealing was verified by x-ray diffraction (XRD, Cu K_α radiation) and transmission electron microscope (TEM, JEM-2100PLUS). The DMA measurements were performed on a TA DMA Q800 in a temperature-ramp mode under the frequency of 1 Hz. The thermal behaviors were measured using a DSC (PerkinElmer 8000) with flowing pure argon gas to prevent oxidation. The original DSC data were used for comparison. For the same glass, ΔC_p, i.e., the difference of the specific heat between
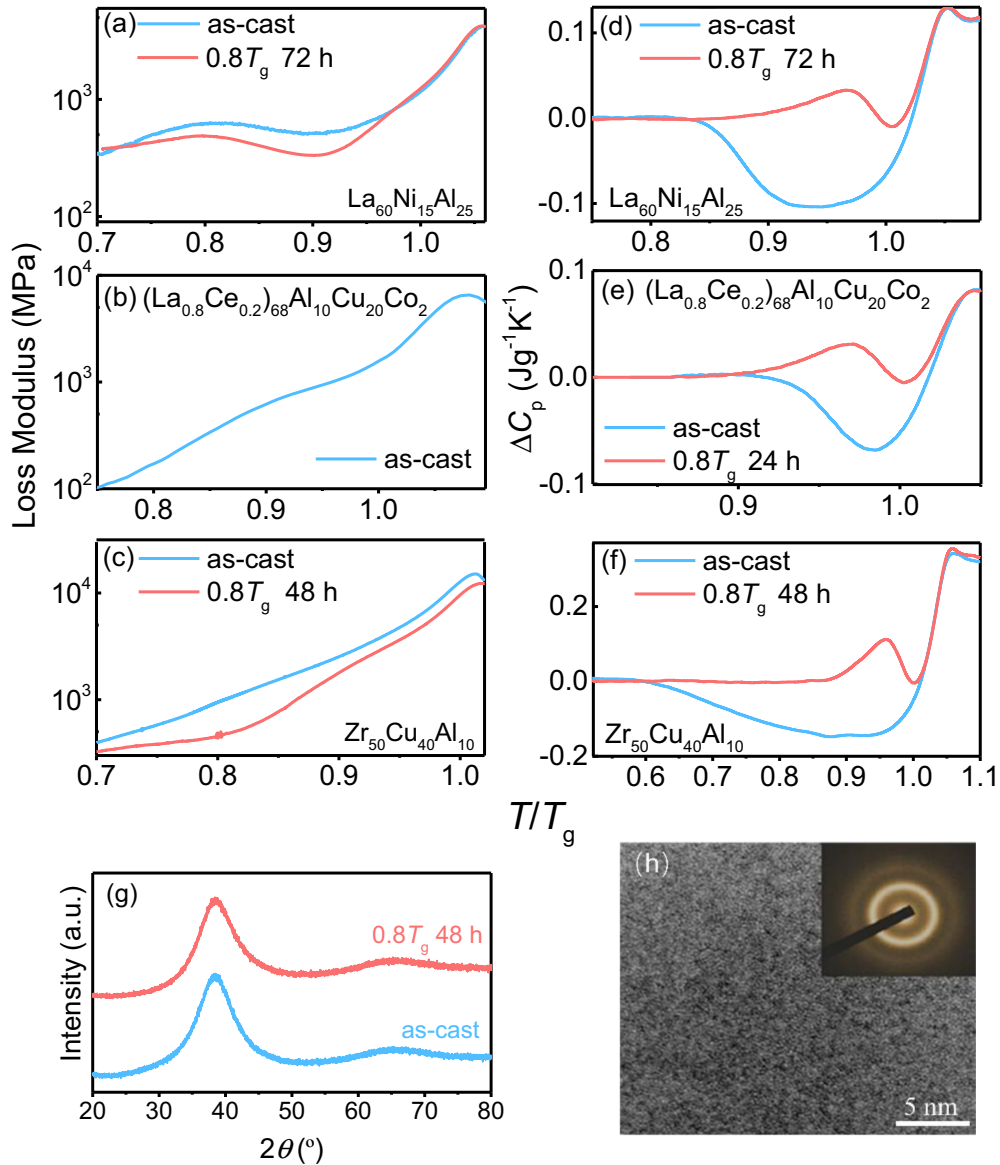
*pengluo@iphy.ac.cn
†whw@iphy.ac.cn

FIG. 1. (a)–(c) Loss modulus E'' at testing frequency $f = 1$ Hz for $La_{60}Ni_{15}Al_{25}$MG, $(La_{0.8}Ce_{0.2})_{68}Al_{10}Cu_{20}Co_2$MG, and $Zr_{50}Cu_{40}Al_{10}$ MG, respectively. (d) Heat-flow profiles of as-cast $La_{60}Ni_{15}Al_{25}$MG and that preannealed at $0.8T_g$ for 72 h at a heating rate of 40 K min^{-1}. (e) Heat-flow profiles of as-cast $(La_{0.8}Ce_{0.2})_{68}Al_{10}Cu_{20}Co_2$MG and that preannealed at $0.8T_g$ for 24 h at a heating rate of 20 K min^{-1}. (f) Heat-flow profiles of as-cast $Zr_{50}Cu_{40}Al_{10}$ MG and that pre-annealed at $0.8T_g$ for 72 h at a heating rate of 80 K min^{-1}. (g) XRD patterns of as-cast $Zr_{50}Cu_{40}Al_{10}$ MG and that annealed at $0.8T_g$ for 48 h. (h) TEM image and corresponding SAED pattern for $Zr_{50}Cu_{40}Al_{10}$ MG annealed at $0.8T_g$ for 48 h.

the glassy state and the liquid state above T_g is the same, they can collapse at both the low-temperature glassy state and the high-temperature liquid state without any normalization (see Fig. 1). We separated the DSC curves (in Figs. 2–5) to make the prepeaks clearer and the offsets along the ΔC_p axis are provided.

III. RESULTS AND DISCUSSION

Figures 1(a)–1(c) show the loss modulus E'' of the three MGs, where their β-relaxations behave differently. The β-relaxation appears as a pronounced peak for $La_{60}Ni_{15}Al_{25}$MG, a hump for $(La_{0.8}Ce_{0.2})_{68}Al_{10}Cu_{20}Co_2$MG,

and a tail of α-relaxation for $Zr_{50}Cu_{40}Al_{10}$ MG. As the samples are annealed below T_g for a prolonged period of time, only intensity decrease of the β-relaxation is observed [Figs. 1(a) and 1(c)].

In contrast to DMA, the DSC measurements provide a more sensitive approach for probing the complex dynamics in glasses, especially on the evolution of the β-relaxation upon applied treatments such as preannealing. Figures 1(d)–1(f) show the heat-flow profiles of the as-cast and the preannealed MGs. The as-cast samples exhibit broad exothermic peaks below T_g, which is generally attributed to an irreversible structural relaxation associated with the annihilation of free volume or other structural defects [20] and the percolation
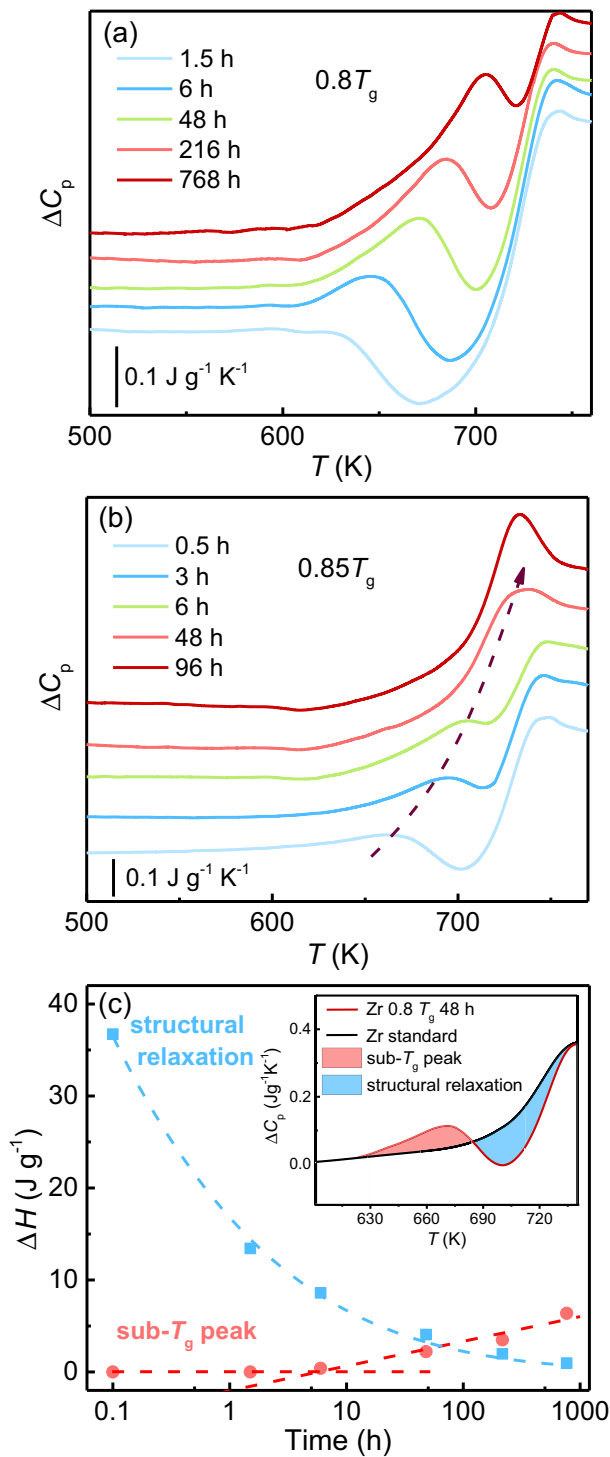
FIG. 2. (a), (b) Heat-flow profiles at a heating rate of 80 K min^{-1} of Zr$_{50}$Cu$_{40}$Al$_{10}$ MG preannealed at $0.8T_g$ and $0.85T_g$ for different times. Offsets along the ΔC_p axis are applied. (c) Enthalpy values of sub-T_g peak and structural relaxation process of Zr$_{50}$Cu$_{40}$Al$_{10}$ MG as a function of annealing time; the inset is a schematic of the calculation of enthalpy values of sub-T_g peak and structural relaxation process.

of flow units [21]. Besides, β-relaxation is often ascribed to the tail of this structural relaxation at the low-temperature side of the broad exothermic peak [22–24]. However, for all three preannealed MGs with different dynamic features in
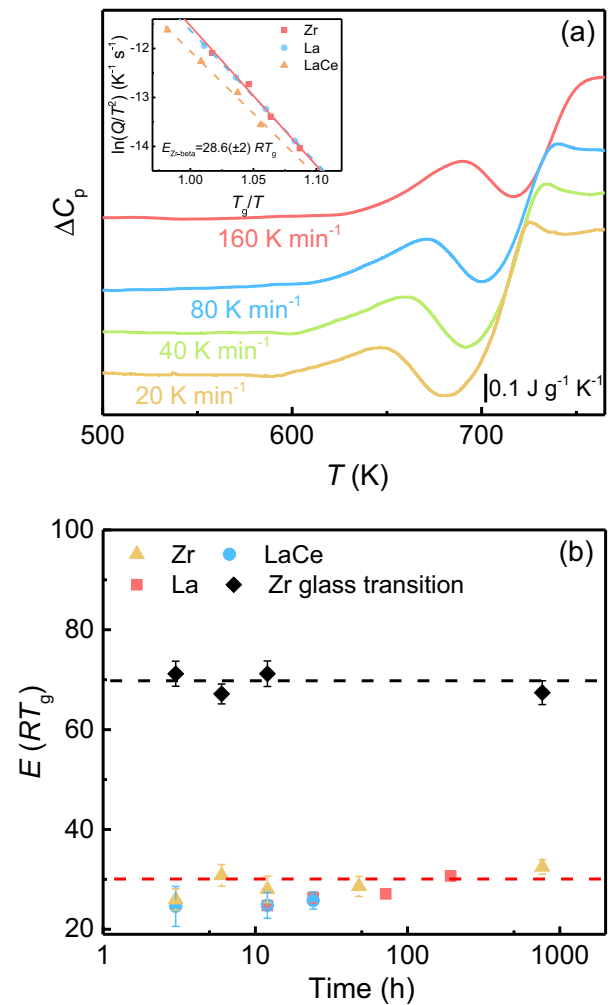

FIG. 3. (a) Heat-flow profiles of Zr$_{50}$Cu$_{40}$Al$_{10}$ MG preannealed at $0.8T_g$ for 48 h at heating rates of 20, 40, 80, and 160 K min^{-1}. Offsets along the ΔC_p axis are applied. Inset: Kissinger plot of $\ln(Q/T_p^2)$ as a function of T_g/T_p. (b) The activation energy of the sub-T_g peak of La$_{60}$Ni$_{15}$Al$_{25}$MG, (La$_{0.8}$Ce$_{0.2}$)$_{68}$Al$_{10}$Cu$_{20}$Co$_2$MG, Zr$_{50}$Cu$_{40}$Al$_{10}$ MG, and the glass transition process of Zr$_{50}$Cu$_{40}$Al$_{10}$ MG as functions of the annealing time. The black dashed line is for the glass-transition process of Zr$_{50}$Cu$_{40}$Al$_{10}$ MG. The red dashed line corresponds to the activation energy of the broad exothermic peak in as-cast Zr-based MG [23].

their mechanical-loss spectra, the exothermic peak disappears and instead, an endothermic peak is observed. Here, this endothermic peak is termed as the sub-T_g peak. As shown in Figs. 1(d)–1(f), for La$_{60}$Ni$_{15}$Al$_{25}$MGs annealed at $0.8T_g$ for 72 h, (La$_{80}$Ce$_{20}$)$_{68}$Al$_{10}$Cu$_{20}$Co$_2$MGs annealed at $0.8T_g$ for 24 h, and Zr$_{50}$Cu$_{40}$Al$_{10}$ MGs annealed at $0.8T_g$ for 48 h, their sub-T_g peaks always appear at the onset of near $0.9T_g$ with a peak temperature of about $0.96T_g$. All the XRD patterns, TEM images, and the selected area electron diffraction (SAED) patterns demonstrate that the annealed samples are fully amorphous without any visible crystalline phases [Figs. 1(g) and 1(h)]. Therefore, the result indicates that the observed distinct sub-T_g peak, arising from the long-time annealing, is an intrinsic feature of glass relaxation, not crystallization.
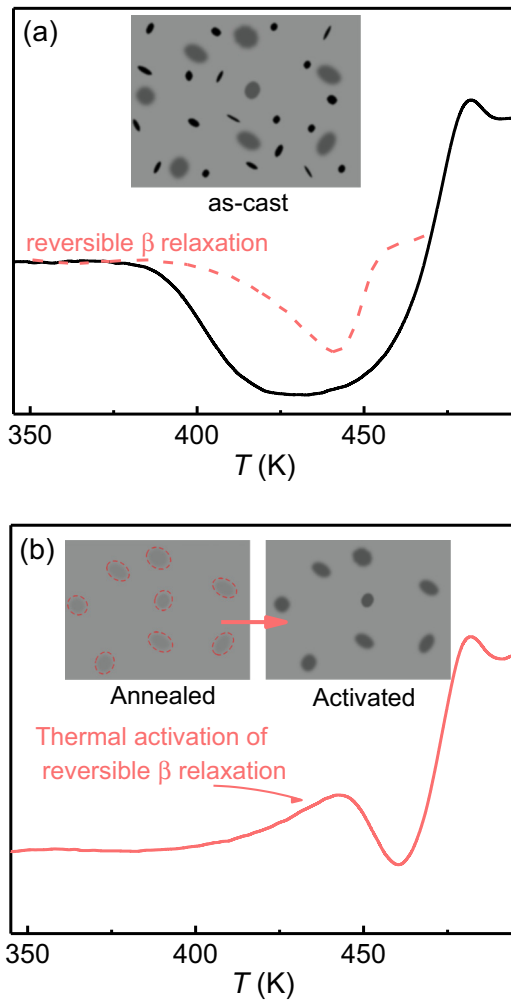
FIG. 4. Schematic depictions of the irreversible and reversible β-relaxation of MGs in different states. (a) In the as-cast sample, many intrinsic flow units (gray balls) and defectlike flow units (dark spots) are frozen. The red dashed line schematically represents the reversible β-relaxation. (b) In the annealed sample, defectlike flow units disappear because of the irreversible β-relaxation and intrinsic flow units relax to low-energy state (light gray balls in red dashed circles) through the occurring of reversible β-relaxation. In the activated sample, the reversible β-relaxation is activated leading to the recovery of the relaxed intrinsic flow units (gray balls). The thermal activation process of reversible β-relaxation leads to the sub-T_g peak of preannealed MG upon heating.

In fact, similar sub-T_g peaks have been observed in other glassy systems such as amorphous water [25], polymeric glasses [26], oxide glasses, and selenide glasses [27]. The sub-T_g peak in amorphous water was attributed to the relaxation of localized defects of the Bjerrum type in ices [26]. Yue and Angell [26] compared the sub-T_g peaks of amorphous water and hyperquenched inorganic glasses and suggested its origin as a "shadow" of the real glass transition. A series of researches on the sub-T_g peak in MGs and molecular glasses suggests that it is associated with the kinetic activation of β-relaxation [28]. The sub-T_g peak observed in the long-term aging of selenide is taken as a result of the dense region of the Se backbone coalescing with the surrounding noncompacted
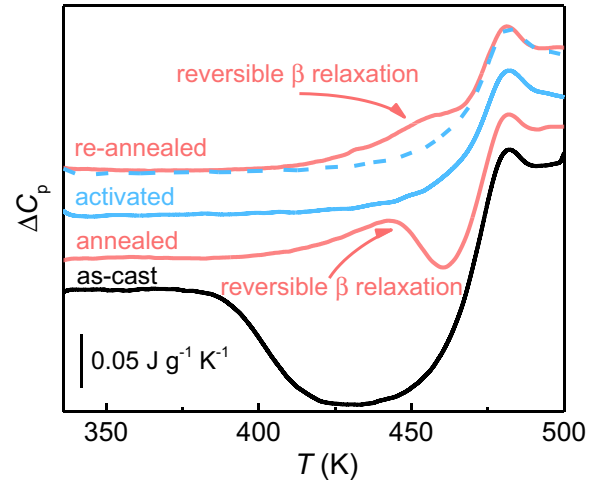

FIG. 5. Heat-flow profiles of $La_{60}Ni_{15}Al_{25}$ MG after different treatments reveal the reproducibility of sub-T_g peak. Offsets along the ΔC_p axis are applied for clarity. The annealed sample is obtained by preannealing at $0.8T_g$ for 72 h. The activated sample is obtained by heating the annealed sample to $0.96T_g$ at 40 K min^{-1} and keeping there for 0.5 min, then cooling down at 100 K min^{-1}; the reannealed sample is obtained by annealing the activated sample at $0.8T_g$ for another 72 h. The sub-T_g peak of the annealed sample disappears after the activation process at $0.96T_g$ for 0.5 min (the solid and dashed blue curves) and can be reproduced by annealing again the activated sample.

regions [27]. Although the underlying mechanism of this universal phenomenon remains debatable, it is widely accepted that the sub-T_g peak in DSC is a localized dynamic mode related to the glass transition.

To understand the features of this universal sub-T_g peak and its correlation with the relaxation dynamics in MGs, the samples were annealed at various temperatures for a prolonged period of time over 700 h. Figures 2(a) and 2(b) present the DSC curves of $Zr_{50}Cu_{40}Al_{10}$ samples preannealed at $0.8T_g$ and $0.85T_g$ for various periods of time. Upon annealing at $0.8T_g$, a sub-T_g peak appears after an annealing time of 6 h, followed by an exothermic peak, suggesting that a localized structural recovery process occurs before the typical structural relaxation process. With increasing the annealing time at $0.8T_g$, the onset temperature of the sub-T_g peak remains unchanged, while the peak position shifts towards higher temperature accompanied by an increase of the peak intensity, exhibiting a tendency to merge with the glass transition. At $0.85T_g$, this merging is observed within the experimental time [Fig. 2(b)], where the sub-T_g peak appears after annealing for just 0.5 h and becomes a shoulder of glass transition at 48 h. It fully merges with the glass transition and becomes an overshoot above T_g after a 96-h annealing.

The enthalpy values of the sub-T_g peak and the structural relaxation were then compared. As shown in the inset of Fig. 2(c), the DSC profile of a standard sample obtained by cooling from $T_g + 40$ K at a rate of 100 K min^{-1} was taken as a reference; the areas enveloped by the sub-T_g peak of the annealed sample and the standard sample (pink area), as well as that of the exothermic peak (blue area), were calculated and plotted as a function of the annealing time [Fig. 2(c)].

In the initial stage of annealing at $0.8T_g$, structural relaxation is dominant. With the increase of annealing time, the sub-T_g peak appears and eventually overwhelms the structural relaxation after around 50 h [Fig. 2(c)]. These observations suggest that the sub-T_g peak is a precursor of the glass-transition overshoot, and the evolution of the sub-T_g peak in annealing shares the similarity of the transition from β- to α-relaxations. On the other hand, β-relaxation can also be regarded as a precursor of α-relaxation and the locus of β-relaxation can be theoretically predicted from the information of its corresponding α-relaxation [11,29,30]. From the perspective of energy landscape theory, the β-relaxation is a reversible event, hopping across the sub-basins confined within an inherent megabasin, while α-relaxation is an irreversible event jumping across the megabasins [6,7,31]. Focusing on the thermal and mechanical activation processes, the β-relaxation is initially activated mainly within the confined flow units, whereas later the cooperation of β-relaxations corresponds to the percolation of the flow units, entailing large-scale irreversible atomic rearrangements associated with α-relaxation [4,32,33]. Therefore, it is reasonable to relate the sub-T_g peak to β-relaxation.

To further study the origin of the sub-T_g peak, the activation energy of the sub-T_g peak and glass-transition process is measured. Figure 3 shows the heating-rate dependent (Q-dependent) DSC profiles for MGs annealed at $0.8T_g$ for 48 h. It is clearly shown that the sub-T_g peak temperature (T_p) increases with Q. The dependence of Q on the reciprocal temperature for both processes can be well fitted by the Kissinger law, $\frac{d \ln(Q/T_p^2)}{d(1/T_p)} = -\frac{E}{R}$, where R is the gas constant and E is the activation energy [34]. The inset in Fig. 3(a) plots $\ln(Q/T_p^2)$ as a function of T_g/T_p for the three annealed MGs, where the value of T_g is taken as the one measured at $Q = 40$ K min^{-1}. The fits by Kissinger law derive activation energy of $E \approx 28.6(\pm 2)RT_g$ for the three samples. Figure 3(b) shows the E of the sub-T_g peak of the three different MGs as a function of annealing time at $0.8T_g$. The data for the glass transition of $Zr_{50}Cu_{40}Al_{10}$ MGs, obtained in the same way, are shown for comparison. The red dashed line represents the E for the onset temperature of the broad exothermic peak in the as-cast Zr-based MGs [24]. The E of the sub-T_g peak in the annealed MGs is consistent with that of the broad exothermic peak in the as-cast MGs, both in agreement with the empirical value of $26RT_g$ for β-relaxation in MGs [6,11], further confirming that the sub-T_g peak is essentially related to the β-relaxation.

Both the sub-T_g peak in the annealed MGs and the broad exothermic peak in the as-cast MGs can be attributed to β-relaxation, while the different features and behaviors of these two phenomena suggest the existence of distinct β-relaxation processes. The β-relaxation in MGs has been related to the flow units which are described as a liquidlike region with faster dynamics [6,21,32]. For the as-cast MG, a large amount of flow units is frozen in the glassy matrix since rapid cooling [21,32]. However, some of the flow units are reversible in response to external stress [35–37], and some are not. The irreversible rearrangements of atoms and subtle structural changes in as-cast MGs during aging, usually ascribed to the annihilation of defects, have been widely observed [38–43]. The flow units in the as-cast MGs are considered to consist

of two parts: the irreversible defectlike parts [small black dots illustrated in the inset of Fig. 4(a)] and the reversible intrinsic parts [gray balls shown in the inset of Fig. 4(b)]. The intrinsic flow units will relax to a fairly low-energy state through the reversible arrangements of atoms confined in the liquidlike regions [4,7,44], while the defectlike flow units will be annihilated and the atoms in such liquidlike regions can irreversibly rearrange to merge with the elastic matrix [4]. The former process is taken as a reversible β-relaxation, while the latter process is identified as an irreversible β-relaxation.

It has been suggested that β-relaxation is superimposed on the broad exothermic peak in the DSC curve of the as-cast MGs [24]. The β-relaxation observed in the as-cast MGs via DSC is the outcome of combined irreversible and reversible β-relaxations. The irreversible β-relaxation is the annihilation process of defectlike flow units, while the reversible β-relaxation is the relaxation process of reversible flow units. Through preannealing of the as-cast samples, the two different β-relaxations can be decoupled. During annealing at $0.8T_g$, both reversible and irreversible β-relaxation processes occur. After 72 h annealing, the irreversible relaxation has been fully activated and the irreversible flow units have been fully depleted. Meanwhile, the reversible β-relaxation is activated in the specific reversible flow units [light gray balls in red dashed circles in the inset of Fig. 4(b)], causing those flow units to relax towards a lower energy state. When heating up the preannealed samples again, the relaxed reversible flow units are reactivated through extra-heat absorption [Fig. 4(b)]. Therefore, the broad exothermic peak disappears, and a pronounced sub-T_g peak appears, corresponding to the activation process of the reversible β-relaxation.

The reproducibility of the sub-T_g peak evidences our argument that the sub-T_g peak originates from the reversible β-relaxation. As shown in Fig. 5, for the $La_{60}Ni_{15}Al_{25}$MG preannealed at $0.8T_g$ for 72 h, the pronounced sub-T_g peak locates at $0.96T_g$, which originates from the reactivation of reversible β-relaxation as illustrated. One can expect that if the reversible β-relaxation is activated in advance, the sub-T_g peak cannot be observed. We heated the preannealed $La_{60}Ni_{15}Al_{25}$MG up to $0.96T_g$ at 40 K min^{-1}, held for 0.5 min, and then cooled down to room temperature at 100 K min^{-1}. The resulting sample is termed as the activated. When heating the activated, the sub-T_g peak indeed disappeared as expected. Interestingly, when we reannealed the activated sample at $0.8T_g$ for another 72 h, the sub-T_g peak was reproduced, confirming the existence of reversible β-relaxation. The reproduced sub-T_g peak is not as pronounced as before and its peak position slightly shifts to a higher temperature, which probably results from the effect of aging while annealing at $0.96T_g$.

The intrinsic β-relaxation in MGs is generally recognized to be reversible because it is a potential activation of nanoscale flow events confined by surrounding atoms [44]. Our result indicates that the β-relaxation detected by DMA is the superposition of irreversible and reversible β-relaxation processes. The different behaviors of β-relaxations determined by DMA and DSC mainly result from the interplay of irreversible and reversible β-relaxations. Compared with DMA, DSC measurements can trace the activation process of β-relaxation more sensitively. The reproducibility and

evolution of reversible β-relaxation shows many phenomeno-logical similarities with the overshoot of α-relaxation, con-firming that the reversible β-relaxation is a localized glass transition [29].

The identifying of irreversible and reversible β-relaxation can deepen our understanding of relaxation and the aging of MGs. For as-cast MGs, the irreversible β-relaxation plays a dominant role in the initial stage of aging because various flow units are frozen during the quenching process. It is the irreversible β-relaxation that leads to the irreversible change of properties. For example, annealing the as-cast MGs below T_g leads to the irreversible increase in the elastic modulus [45], and the annealing of the as-cast Zr-based MGs at $0.85T_g$ results in dramatic homogenization after only 30 min [46]. Recent simulations and experiments on microscopic dynam-ics also indicate the existence of irreversible and reversible secondary relaxations [19,47,48]. In simulations of thermally activated deformation, two deformation modes, one localized and the other cascade were observed [19], and the localized process is nearly unchanged with cooling rate, similar to the reversible β-relaxation. The cascade deformation occurs more frequently in the fast-quenched system like the irreversible β-relaxation. The sub-T_g peak has also been observed in an ultrastable MG produced by physical vapor deposition [49] and antiaging was found in such ultrastable MGs, which may be a result of the activation of reversible β-relaxation [47]. The microscopic dynamics of a quenched $Pd_{77}Si_{16.5}Cu_{6.5}$MG studied by x-ray photon correlation spectroscopy also sug-gested that the atomic-scale dynamics is a result of the in-terplay between the irreversible process related to the release of residual stresses and the reversible process of medium-range ordering associated with the localized relaxation of the liquidlike regions [48].

IV. CONCLUSION

We show DSC measurement is an efficient way to probe the intrinsic β-relaxation, and isothermal annealing can separate the dynamic relaxation modes of metallic glass. We find that the localized and secondary relaxation includes both irreversible and reversible parts, and the isothermal anneal-ing below T_g can induce decoupling of the irreversible and reversible β-relaxation processes. The former, appearing as a broad exothermic peak on the DSC profiles, is related to the defectlike flow units and more frequently observed in highly unstable as-cast MGs, while the latter, appearing as an endothermic sub-T_g peak, originates from the intrinsic flow units and becomes increasingly pronounced upon annealing. The identification of irreversible and reversible β-relaxation is helpful for the understanding of the relaxation and the aging of MGs.

[1] I. M. Hodge, Science **267**, 1945 (1995).

[2] B. Ruta, E. Pineda, and Z. Evenson, J. Phys.: Condens. Matter **29**, 503002 (2017).

[3] P. G. Debenedetti and F. H. Stillinger, Nature (London) **410**, 259 (2001).

[4] Z. Wang, B. A. Sun, H. Y. Bai, and W. H. Wang, Nat. Commun. **5**, 5823 (2014).

[5] P. Wen, D. Q. Zhao, M. X. Pan, W. H. Wang, Y P. Huang, and M. L. Guo, Appl. Phys. Lett. **84**, 2790 (2004).

[6] H. B. Yu, W. H. Wang, H. Y. Bai, Y. Wu, and M. W. Chen, Phys. Rev. B **81**, 220201(R) (2010).

[7] J. S. Harmon, M. D. Demetriou, W. L. Johnson, and K. Samwer, Phys. Rev. Lett. **99**, 135502 (2007).

[8] T. Ichitsubo, E. Matsubara, T. Yamamoto, H. S. Chen, N. Nishiyama, J. Saida, and K. Anazawa, Phys. Rev. Lett. **95**, 245501 (2005).

[9] H. B. Yu, K. Samwer, Y. Wu, and W. H. Wang, Phys. Rev. Lett. **109**, 095508 (2012).

[10] H. B. Yu, X. Shen, Z. Wang, L. Gu, W. H. Wang, and H. Y. Bai, Phys. Rev. Lett. **108**, 015504 (2012).

[11] H. B. Yu, W. H. Wang, and K. Samwer, Mater. Today **16**, 183 (2013).

[12] J. D. Stevenson and P. G. Wolynes, Nat. Phys. **6**, 62 (2010).

[13] P. Luo, Z. Lu, Z. G. Zhu, Y. Z. Li, H. Y. Bai, and W. H. Wang, Appl. Phys. Lett. **106**, 031907 (2015).

[14] H. B. Yu, W. H. Wang, H. Y. Bai, and K. Samwer, Natl. Sci. Rev. **1**, 429 (2014).

[15] Z. Wang, H. B. Yu, P. Wen, H. Y. Bai, and W. H. Wang, J. Phys.: Condens. Matter **23**, 142202 (2011).

[16] P. Luo, Z. Lu, Y. Z. Li, H. Y. Bai, P. Wen, and W. H. Wang, Phys. Rev. B **93**, 104204 (2016).

[17] P. Luo, M. X. Li, H. Y. Jiang, P. Wen, H. Y. Bai, and W. H. Wang, J. Appl. Phys. **121**, 135104 (2017).

[18] P. Luo, P. Wen, H. Y. Bai, B. Ruta, and W. H. Wang, Phys. Rev. Lett. **118**, 225901 (2017).

[19] Y. Fan, T. Iwashita, and T. Egami, Phys. Rev. Lett. **115**, 045501 (2015).

[20] A. Vandenbeukel and J. Sietsma, Acta Metall. Mater. **38**, 383 (1990).

[21] Z. Wang and W. H. Wang, Natl. Sci. Rev. **6**, 304 (2018).

[22] H. S. Chen and E. Coleman, Appl. Phys. Lett. **28**, 245 (1976).

[23] J. C. Lee, Intermetallics **44**, 116 (2014).

[24] Y. H. Liu, T. Fujita, D. P. B. Aji, M. Matsuura, and M. W. Chen, Nat. Commun. **5**, 3238 (2014).

[25] G. P. Johari, A. Hallbrucker, and E. Mayer, Nature (London) **330**, 552 (1987).

[26] Y. Yue and C. A. Angell, Nature (London) **427**, 717 (2004).

[27] P. Chen, P. Boolchand, and D. G. Georgiev, J. Phys.: Condens. Matter **22**, 065104 (2010).

[28] Z. Evenson, S. E. Naleway, S. Wei, O. Gross, J. J. Kruzic, I. Gallino, W. Possart, M. Stommel, and R. Busch, Phys. Rev. B **89**, 174204 (2014).

[29] K. L. Ngai and M. Paluch, J. Chem. Phys. **120**, 857 (2004).

[30] S. Capaccioli, M. Paluch, D. Prevosto, L. M. Wang, and K. L. Ngai, J. Phys. Chem. Lett. **3**, 735 (2012).

[31] F. H. Stillinger, Science **267**, 1935 (1995).

[32] W. H. Wang, Y. Yang, T. G. Nieh, and C. T. Liu, Intermetallics **67**, 81 (2015).

[33] Q. Wang, S. T. Zhang, Y. Yang, Y. D. Dong, C. T. Liu, and J. Lu, Nat. Commun. **6**, 7876 (2015).

[34] H. E. Kissinger, Anal. Chem. **29**, 1702 (1957).

[35] J. C. Ye, J. Lu, C. T. Liu, Q. Wang, and Y. Yang, Nat. Mater. **9**, 619 (2010).

[36] A. S. Argon, Acta Metall. **27**, 47 (1979).

[37] M. L. Falk and J. S. Langer, Annu. Rev. Condens. Matter Phys. **2**, 353 (2011).

[38] A. R. Yavari, A. L. Moulec, A. Inoue, N. Nishiyama, N. Lupu, E. Matsubara, W. J. Botta, G. Vaughan, M. D. Michiel, and Å. Kvick, Acta Mater. **53**, 1611 (2005).

[39] R. Brüning and J. O. Ström-Olsen, Phys. Rev. B **41**, 2678 (1990).

[40] P. Yunker, Z. Zhang, K. B. Aptowicz, and A. G. Yodh, Phys. Rev. Lett. **103**, 115701 (2009).

[41] J. Bednarcik, C. Curfs, M. Sikorski, H. Franz, and J. Z. Jiang, J. Alloys Compd. **504**, S155 (2010).

[42] A. I. Taub and F. Spaepen, Acta Metall. **28**, 1781 (1980).

[43] W. Li, H. Bei, Y. Tong, W. Dmowski, and Y. F. Gao, Appl. Phys. Lett. **103**, 171910 (2013).

[44] W. H. Wang, Prog. Mater. Sci. **106**, 100561 (2019).

[45] J. Hachenberg, D. Bedorf, K. Samwer, R. Richert, A. Kahl, M. D. Demetriou, and W. L. Johnson, Appl. Phys. Lett. **92**, 131911 (2008).

[46] Y. H. Liu, D. Wang, K. Nakajima, W. Zhang, A. Hirata, T. Nishi, A. Inoue, and M. W. Chen, Phys. Rev. Lett. **106**, 125504 (2011).

[47] M. Lüttich, V. M. Giordano, S. Le Floch, E. Pineda, F. Zontone, Y. Luo, K. Samwer, and B. Ruta, Phys. Rev. Lett. **120**, 135504 (2018).

[48] V. M. Giordano and B. Ruta, Nat. Commun. **7**, 10344 (2016).

[49] H. B. Yu, Y. Luo, and K. Samwer, Adv. Mater. **25**, 5904 (2013).